PHYS 304 Final Project

Nathaniel Ruhl*
Haverford College
(Dated: April 29, 2022)

A simplified, semi-analytical model of a horizon crossing is introduced in order to provide insight into the numerical methods involved in horizon crossing analysis. This report considers the transmission of X-rays from a celestial source that penetrate a hydrostatically balanced, isothermal atmosphere governed by an exponential model of atmospheric mass density. Adaptive integration of optical depth along a telescopic line of sight suggests that a step size of ∼17 km is optimal when analyzing a horizon crossing of 4.0 keV photons for a satellite in a circular orbit with an altitude of 420 km above Earth. A method to solve for atmospheric parameters of an exponential atmosphere is introduced. The total effective photoelectric cross section of atmospheric constituents and the atmosphere's surface-level density can be solved directly, while atmospheric scale height can be solved with a nonlinear root-finding algorithm such as the Newton-Raphson method. Extensions for future work are discussed in the appendices, which include a set of non-dimensional parameters and a formulation of X-ray attenuation as function of time.

1. INTRODUCTION

Occultations of stellar sources have been used for decades to remotely sense planetary atmospheres in a wide range of energy band-passes [1–3]. By analyzing the attenuation (absorption, scattering, refraction, etc.) of radiation in a planetary atmosphere, scientists can measure different aspects of the atmosphere's composition and structure in a variety of altitude ranges. Smith and Hunten [2] provide a concise review of absorptive occultation techniques and data reduction methods, and discusses how they have been used to study planetary atmospheres. Occultations of X-ray point sources are particularly useful for measuring the neutral density of an atmosphere, since the emitted radiation is not spread into a wide beam as it goes through a planet's atmosphere [1]. Additionally, soft X-rays (∼1 – 10 keV) are solely absorbed by atmospheric constituents via the photo-electric effect [3]. This means that other attenuation processes, such as scattering, do not need to be modeled when analyzing an x-ray occultation [4]. X-rays are absorbed by the innermost and most tightly bound K and L shell electrons, which implies that absorption is independent of ionization state, electron state, and chemical bonds of atmospheric gases [3]. For these reasons, attenuation of soft X-rays in a planetary atmosphere is highly predictable and can be modeled by the differential equation

$$\frac{dI}{dx} = -\gamma I, \tag{1}$$

where I is the intensity of the source, γ is a coefficient of interaction between the radiation and the attenuating medium, and x is the width of the medium, where a differential cross section of the attenuating medium has a surface normal vector parallel to the direction that the radiation travels. Eq. (1) means that the attenuating medium removes particles from the incoming beam at a rate that is proportional to the incoming flux of particles, I. The solution to Eq. (1), known as Beer's law, is given by

$$I(x) = I(x_0)e^{-\gamma\Delta x}, \tag{2}$$

where $\Delta x = x - x_0$ is the width of the attenuating medium over which γ is a constant. For soft X-rays in a planetary atmosphere, $\gamma = \gamma(E, x) = \sigma(E)\rho(x)$, where $\sigma(E)$ is the absorption cross section of the medium, which depends on the energy E of the incoming radiation, and $\rho(x)$ is the density of the medium along the direction perpendicular to the radiation's motion.

Recently, it has been showed that occultations, and "horizon crossings" in particular, can can also be used for navigation, in adittion to atmospheric science Ruhl et al. [5]. Horizon crossings are a specific kind of "rising" occultation, where the transmission of intensity from the source is observed to rise from 0% to 100%, whereas in a traditional occultation, transmission starts at 100% and falls to 0%. The atmospheric science problem and the navigational problem are two sides of the same coin. In the former, the state of the satellite is assumed to be known perfectly, and the occultation is used to determine an unknown parameter in the planet's atmospheric model. In the navigational problem, the atmosphere is assumed to be known, and the occultation is used to determine the position of the satellite in orbit. Ruhl et al. [5] have shown that a horizon crossing around Earth can provide the International Space Station (ISS) with an "in-track" measurement of less than 1 km depending on the brightness of the X-ray source. The Horizon Crossing Navigational Method (HCNM) has the potential to provide high-precision measurements to a navigational filter for autonomous navigation around distant planets [6].

Another reason that horizon crossings are so exciting is that "dual use" can be achieved with an X-ray detector that observes horizon crossings. Upon arrival at a

*Electronic address: nruhl@haverford.edu

planetary orbit, horizon crossings can be used to both measure the planet's atmosphere and to perform navigation, iteratively improving both solutions as the satellite performs multiple sequential horizon crossings. In this paper, we will consider a simplified, semi-analytical horizon crossing that will provide insight into the numerical techniques used in HCNM. Although the methods presented in this paper are conducted for a specific model orbit around Earth, these numerical methods can easily be applied to an arbitrary planet with an exponential atmosphere.

2. GEOMETRY OF A TWO-DIMENSIONAL HORIZON CROSSING

Figure 1 shows a diagram of a horizon crossing in which there are two satellites observing horizon crossings of two different sources. One of the telescopic lines of sight is looking $\sim 20°$ out of the orbital plane, while the other telescope observes a source that is "in the plane of the orbit". When analyzing a horizon crossing, it is important to consider the out-of-plane angle of the source, as well as the exact orbital model and the shape of the orbited planet as an ellipsoid. In this paper however, we consider the horizon crossing of a source that is "in" the plane of the orbit, conducted by a satellite in a perfectly circular orbit about a planet that is modeled as a sphere. Figure 2 shows a diagram of the simplified two-dimensional horizon crossing considered in this paper.

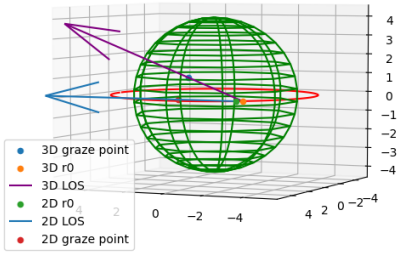

FIG. 1: Diagram of a horizon crossing which shows both a three-dimensional horizon crossing and an idealized two-dimensional horizon crossing.

Figure 3 shows the geometry that is used to derive the analytical formulas involved in a horizon crossing. This is also known as a "limb-looking" geometry in remote sensing [7].

In Figure 3, R is radius of planet, H is altitude of the orbit, and $R_{orbit} = R + H$ is the radius of the orbit. $h = h(t)$ is the altitude of the "tangent point" of the line of sight, or simply tangent altitude, which will be defined in Eq. (6). The constant angle θ is defined based on the

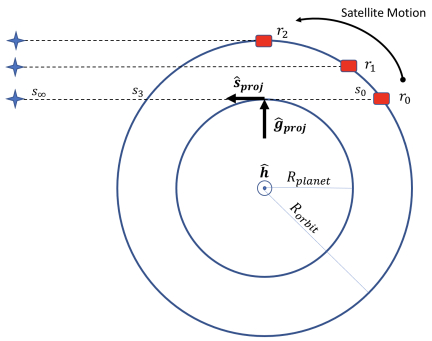

FIG. 2: Simplified, "two-dimensional" horizon crossing. $\hat{\mathbf{s}}_{\mathbf{proj}}$ is the direction vector of the source projected into the plane of the orbit. The orbital plane is defined by the normal vector $\hat{\mathbf{h}}$, which is also known as the orbital pole vector. $\hat{\mathbf{g}}_{\mathbf{proj}}$ is the direction vector to the telescopic "grazing point", which is projected into the orbital plane.

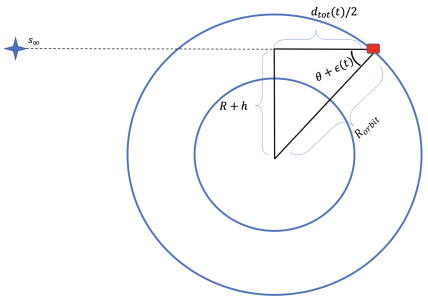

FIG. 3: Geometry for deriving the analytical formulas of a simplified two-dimensional horizon crossing.

ratio of the planet's radius to the satellite's orbital radius as follows:

$$\sin(\theta) = \frac{R}{R_{orbit}}. \tag{3}$$

The "elevation angle" as function of time throughout the horizon crossing is defined as $\epsilon(t) = \omega t$ where ω is the satellite's angular velocity, $\omega = 2\pi/T$. The period of the satellite's circular orbit is determined by Kepler's Third Law:

$$T^2 = \frac{4\pi^2 R_{orbit}^3}{GM}, \tag{4}$$

where G is the gravitational constant, M is the mass of the planet, and R_{orbit} is the orbital radius.

Throughout a horizon crossing, the elevation angle spans from $\epsilon_0 = 0$ to $\epsilon_f = \frac{\pi}{2} - \theta$. The total duration of the horizon crossing, t_f, is determined by dividing ϵ_f by the satellite's angular velocity,

$$t_f = \frac{\epsilon_f}{\omega}. \quad (5)$$

The tangent altitude of the telescopic line of sight, $h(t)$, is given by the equation

$$h(t) = R_{orbit}\sin(\theta + \epsilon(t)) - R. \quad (6)$$

Using the triangle defined in Figure 3, the total length of the line of sight through the atmosphere is

$$d_{tot}(t) = 2 * \sqrt{R_{orbit}^2 - (R + h(t))^2}, \quad (7)$$

where we assume that X-ray attenuation is negligible at altitudes larger than the satellite's orbital altitude, H. At a time, t, there is a one-to-one relationship between the distance of a point along the line of sight, x, and the altitude of the point above the planet's surface, z. The forward and backward transformations between x and z are given in Eq. (8) and Eq. (9):

$$z(x,t) = \sqrt{(R + h(t))^2 + \left(\frac{d_{tot}(t)}{2} - x\right)^2} - R \quad (8)$$

$$x(z,t) = \frac{d_{tot}(t)}{2} - \sqrt{(R + z)^2 - (R + h(t))^2}. \quad (9)$$

In order to represent this one-to-one relationships, we introduce the generalized coordinate/function $\xi(t)$ of unit length, which represents the position of a point on the telescopic line of sight at the time t, whether it be in terms of x or z.

$$\xi(t) : (R + h(t))^2 + \left(\frac{d_{tot}(t)}{2} - x\right)^2 = (R + z)^2 \quad (10)$$

3. MODEL OF X-RAY ABSORPTION

For an isothermal atmosphere of a constant chemical make-up, hydrostatic equilibrium enforces that density follows an exponential profile of the form

$$\rho(z) = \rho_0 e^{-\frac{(z - z_0)}{L}} \quad (11)$$

where z is altitude above the surface, z_0 is the altitude at which the atmospheric scale height L is defined, and ρ_0 is the density at the altitude z_0. The scale height is defined as the altitude required for density to drop by a factor of 1/e. In this paper, we will consider $z_0 = 0$ for simplicity. Although a single exponential model is a vast over-simplification of atmospheric dynamics, more realistic atmospheric models are often made from superpositions of multiple exponential laws in different ranges of altitude. In this paper, we will consider the simple exponential density model given in Eq. (11) in order to gain insight into horizon crossings around planets other than Earth where we may not have a more accurate density profile. The form of the solution to Eq. (1) that is used in our analysis is

$$T(E, t_i) = e^{-\tau(E,t_i)} \quad (12)$$

where $T = I/I_0$ is the "transmittance" of X-ray photons of an energy E that make it through a planet's atmosphere are detected by the telescope at a time t_i. $\tau(E, t_i)$ is a non-dimensional optical depth which is equal to the integral of photoelectric cross section, $\sigma(E)$, multiplied by atmospheric density, $\rho(z)$, along the entire line of sight,

$$\tau(E, t_i) = 2\int_{\xi_0(t_i)}^{\xi_{tp}(t_i)} \sigma(E)\rho(\xi(t_i))d\xi(t_i). \quad (13)$$

If an optical depth per unit length is introduced, $\gamma(E, \xi(t_i)) = \sigma(E)\rho(\xi(t_i))$, Eq. (13) can be re-written as

$$\tau(E, t_i) = 2\int_{\xi_0(t_i)}^{\xi_{tp}(t_i)} \gamma(E, \xi(t_i))d\xi(t_i) \quad (14)$$

where $\xi_0(t_i)$ represents the start of the telescopic line of sight at the time t_i ($x = 0$ and $z = H$) and $\xi_{tp}(t_i)$ represents the tangent point of the line of sight ($x = d_{tot}(t_i)/2$ and $z = h(t_i)$).

The integral of Eq. (14) is simple to evaluate numerically, since $\xi(t)$ provides a one-to-one relationship between x and z at a single time. If we were to set up the integral to evaluate it analytically with respect to z, it would have the form

$$\tau(E, t_i) = 2\sigma(E)\rho_0 \int_H^{h(t_i)} e^{-\frac{z}{L}} g(z, t_i)dz, \quad (15)$$

where $g(z, t_i)$ transforms the integral step from dx to dz, and is given by the derivative of Eq. (9),

$$g(z, t_i) = \frac{-(R + z)}{\sqrt{(R + z)^2 - (R + h(t_i))^2}}. \quad (16)$$

4. ADAPTIVE LINE OF SIGHT INTEGRATION

4.1. Motivation for adaptive step sizes

Figure 4 shows a plot of transmittance vs. time for 4.0 keV photons. This plot is made for a satellite that is in a

circular orbit around Earth with an altitude of $H = 420$ km. The atmospheric model that is used for Earth has a scale height of $L = 8.5$ km and a surface-level density of $\rho_0 = 0.001225$ g/cm^3. All plots and results in this section are calculated for this orbit, which will be denoted as the "standard LEO" (low-Earth orbit). Figure 5 shows a plot of transmittance as a function of tangent altitude, $h(t)$. The plot of transmittance vs. tangent altitude is a property of a planet's atmosphere, and thus is always the same for satellites in different orbits around the same planet. On the other hand, the transmittance vs. time plot will be different for different orbits around the same planet.

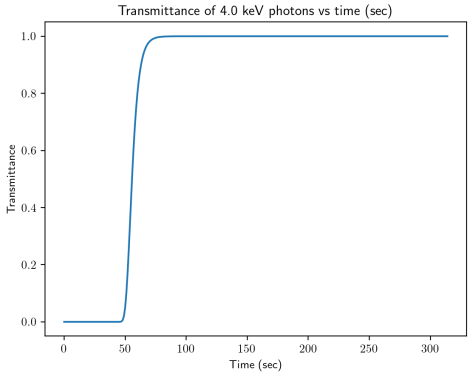

FIG. 4: Transmittance vs. time of 4.0 keV photons for the standard LEO.

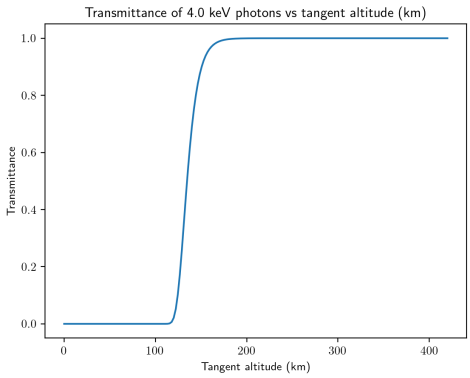

FIG. 5: Transmittance vs. tangent altitude of 4.0 keV photons during a horizon crossing around Earth.

Figure 6 shows a plot of optical depth per km, γ, at different points along the telescopic line of sight, x. The curves correspond to the line of sight at different times during the "interesting" part of the horizon crossing for a range of times when the transmittance is between 0.1 and 0.9.

The area under a curve of γ vs. x is equal to the optical depth, τ, along a telescopic line of sight at a given time. As shown in Figure 6, almost all of the X-ray

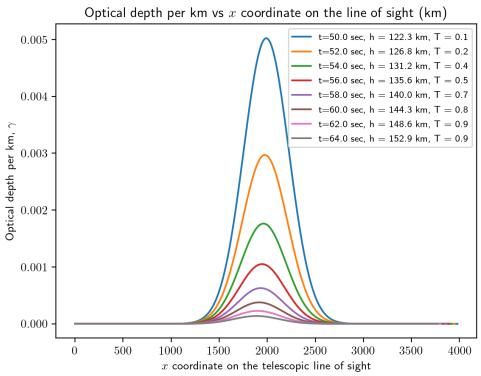

FIG. 6: Plot of optical depth per km, γ, as a function of distance, x, along the telescopic line of sight.

absorption occurs within ± 500 km of the tangent point, even though the total line of sight is $\sim$4000 km long. Figure 7 shows that over 96% of the total absorption occurs within ± 500 km of the tangent point at any time in the horizon crossing.

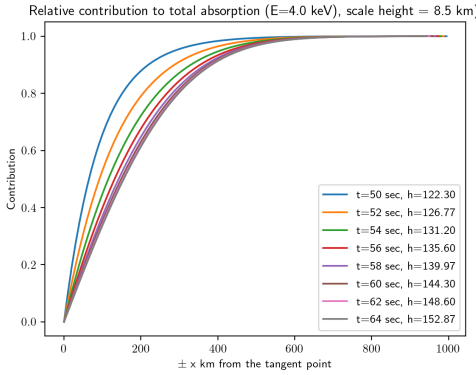

FIG. 7: Relative contribution to the total absorption along a telescope line of sight within $\pm x$ km of the tangent point.

It is important to note that this relationship is specific for 4.0 keV photons penetrating an exponential density model of Earth's atmosphere with a scale height of 8.5 km centered at sea-level, with a sea-level density of $\rho_0 = 0.001225$ g/cm^3. The relationship is different for different exponential models and different energy photons. Determan et al. [3] claim that for an atmospheric model with scale height of $\sim$ 6 km at 100 km tangent altitude, 75% of the absorption occurs within ± 250 km of the tangent point. Our analysis produces very similar results for a scale height of 6 km (and the slight difference is likely due to the fact that our exponential model is centered at a tangent altitude of 0 km, not 100 km).

For this reason, the integral in Eq. (13) can be evaluated accurately and more efficiently by taking larger step sizes near the edges of the telescopic line of sight and smaller step sizes near the center. In this section, we

consider an "adaptive" integration method in order to determine the integration step sizes required to achieve a desired precision when integrating different portions of the line of sight.

In HCNM, Ruhl et al. [5] evaluated Beer's Law with a left-hand Riemann sum of 0.5 km steps. With a programming language that supports vectorization, such as Python, MATLAB, and C++, it is possible to evaluate the optical depth integral with this technique. However, this technique is not possible in all programming languages, and when HCNM is implemented on a flight computer, it may need to run on C, or another lower-level programming language. This is another reason why it is extremely important to understand the step sizes required when integrating the line of sight. Finally, it is important to note that, in the full algorithm of HCNM, the geometrical formulas developed in Section 2 cannot be used. An input orbital model and the source's position in the sky must be used, and the analysis must be done numerically at every time step. However, the *toy model* developed in this paper provides great insight into the algorithm that should be used in the full analysis. Moreover, horizon crossings are often observed when a satellite is in an approximately circular orbit and when the source is only a few degrees out of the plane, so the assumptions in the two-dimensional model are not completely unrealistic.

4.2. Description of Adaptive Quadrature

The method of adaptive integration that we will consider is one kind of "adaptive quadrature". In this method, Simpson's 1/3 and Simpson's 3/8 rules, which approximate the area under a parabola with three and four sample points, respectively, are applied at two levels of refinement in order to estimate the truncation error, ϵ [8]. With Simpson's 1/3 rules, the integrand is approximated by a quadratic over the domain and with Simpson's 3/8 rules, the integrand is approximated by a cubic. As derived in Newman [9], the truncation error for Simpson's rule can be determined by evaluating an integral numerically with a step size of h_1, and then re-evaluating the integral with a smaller step size of $h_2 = h_1/2$. The truncation error, also known as the *Euler-Mclaurin error*, is given by

$$\epsilon = \frac{1}{15}(I(h_2) - I(h_1)). \tag{17}$$

The adaptive quadrature method used in this paper is inspired by pseudo code from Chapra and Canale [8], which is originally based on MATLAB code developed by Cleve Moler (2005). In this method, the first estimate of an integral, I_1, on an interval $x = a$ to $x = b$ with a width of $h_1 = b - a$. The first integral is estimated with Simpson's 1/3 rule as

$$I(h_1) = \frac{h_1}{6}(\gamma(a) + 4\gamma(c) + \gamma(b)), \tag{18}$$

where $c = (b + a)/2$ is the midpoint of the interval. A second estimate of the integral, I_2, is obtained by halving the step size, and evaluating Simpson's rule with four sample points,

$$I(h_2) = \frac{h_2}{6}(\gamma(a) + 4\gamma(d) + 2\gamma(c) + 4\gamma(e) + \gamma(b)), \tag{19}$$

where the points $d = (a + c)/2$ and $e = (c + b)/2$ are the midpoints of the left and right sub-intervals.

An estimate of the error of the integral is $E \approx I(h_2) - I(h_1)$. If E is less than the desired tolerance of the integral, we accept the value of the integral. As derived by Chapra and Canale [8], an even better estimate of the integral, I, can be determined by adding the *Euler-Mclaurin error*, ϵ,

$$I = I(h_2) + \frac{1}{15}(I(h_2) - I(h_1)), \tag{20}$$

which is the value of the integral that is used for the portion of the curve from $x = a$ to $x = b$.

If E is larger than the desired tolerance is not achieved, b replaces c, which means that the upper bound of the integral moves to the center of the old integration domain. This creates a new, smaller integration domain from $x = a$ to $x = b$ on the left-hand side of the original domain. This process of moving the upper bound to the center of the previous integration domain is repeated until the desired tolerance is achieved. Let this iteration be described by the function `qstep()`.

Once E is less than the tolerance, we store the value of the integral, a replaces b, b moves back to the right-most end of the domain, and there is a new interval from $x = a$ to $x = b$ to be integrated. This process is repeated until a, the lower bound of the integral, reaches the upper bound of the integral. Let this iteration be described by the function `quadapt()`. In conclusion, the function `quadapt()` defines an integration domain that has not yet been integrated within the entire integral domain, and `qstep()` iteratively cuts the domain in half until tolerance is achieved. Based on where `qstep()` achieves convergence, a new integration domain will be defined so that it does not include the portion of the domain that was successfully integrated.

4.3. Convergence of Adaptive Quadrature

In the application of adaptive quadrature, a corresponds to $x = 0$ and b corresponds to $x = d_{tot}(t_i)/2$, the full range necessary when integrating the line of sight. Adaptive quadrature as described in Section 4.2 is then performed to reduce the domain size on a sub-interval

until convergence is achieved for a section of the total domain (the total domain is half of the line of sight, as described in Eq. 14). This process is repeated until all section of the total domain is integrated. Figure 8 shows the transmittance curves calculated with adaptive quadrature using three different optical depth tolerances.

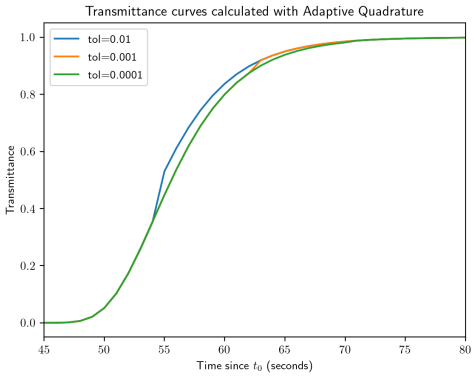

FIG. 8: Transmittance vs time curves calculated using adaptive quadrature with three different tolerance levels.

Since the curves of Figure 8 are not smooth, the adaptive quadrature method should only be used for tolerances less than 10^{-5}. In Figure 9, we consider the fractional difference between the transmittance calculated by adaptive quadrature and the transmittance calculated using gaussian quadrature with 100 quadrature points. This plot shows a range of tolerances from 10^{-5} down to 10^{-9} on the x-axis, and shows that a tolerance of 10^{-7} or 10^{-8} converges and seems to reach machine precision for Python running on Mac OS. Figure 10 shows the runtime of calculating a full transmittance curve (∼320 evaluations of Eq. 13) in Python.

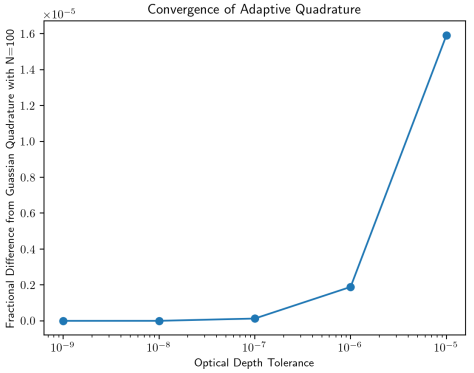

FIG. 9: Estimate of integral error plotted against tolerance used in adaptive quadrature.

The convergence and run-time of adaptive quadrature is not impressive in Python, although this method may be much more efficient in a compiled language. For comparison, the convergence and run-time of Gaussian quadrature are shown in Figures 15 and 16. Figure 15 shows convergence with 10 quadrature points, which takes ∼ 0.26 seconds. As discussed by Newman [9], it is possible to create adaptive quadrature methods that re-use half of the previous integral when cutting the integration step in half, which would provide a significant performance enhancement in an interpreted language like Python.

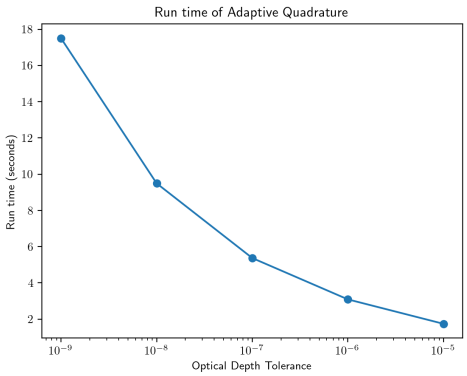

FIG. 10: Run-time of adaptive quadrature for different tolerances.

Although the adaptive quadrature method is not the most time-efficient, it provides insight into the smallest step sizes necessary to achieve the desired optical depth precision. Specifically, the results of the adaptive quadrature method should be considered when creating an integration method to run on a flight computer. Figure 11 shows the optimal step-size identified by adaptive quadrature as a function of distance along the line of sight at $t = 50.0$ seconds from $x = 0$ to the tangent point at $x = d_{tot}/2$.

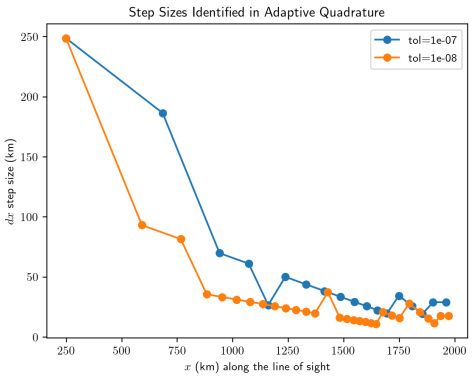

FIG. 11: Optimal step sizes identified in adaptive quadrature for the section of the line of sight with midpoint x plotted on the x-axis. This plot represents the step-size taken for a horizon crossing at $t = 50$ sec of the "standard LEO" previously introduced.

For a tolerance of 10^{-7} the required step size is never smaller than 17 km, while the results for 10^{-8} never step below 8 km. For the "standard LEO" used in this anal-

ysis, step sizes of $\lesssim 17$ km are required near the middle of the line of sight, and seem to achieve machine precision (Python/Mac OS) when using a method such as Simpson's rule. In Python, the calculation of the entire transmittance curve will take $\gtrsim 5$ seconds with the adaptive method, but only $\sim$0.26 seconds for gaussian quadrature with 10 quadrature points. Figure 15 of Appendix A shows that gaussian quadrature with 10 points achieves numerical precision.

5. NONLINEAR EQUATION SOLVING

Beer's Law, $T = e^{-\tau}$, can be inverted to solve for one constant, $\sigma(E)$, ρ_0, or L, provided that the other two are known. It turns out that $\sigma(E)$ and ρ_0 can be solved semi-analytically by re-arranging Beer's law, but since Beer's Law is nonlinear in L, it must be solved with an iterative *root-solving* technique. In this section, we will simulate X-ray transmittance data and use the Newton-Raphson method to solve for L when $\sigma(E)$ and ρ_0 are well defined.

Let $T_i = I_i/I_0$ be the transmittance of X-rays photons observed by a telescope at the time t_i after the start of a horizon crossing. For the exponential atmosphere, Beer's law reduces to

$$T_i = e^{-2\sigma(E)\rho_0\zeta(t_i,L)}, \tag{21}$$

where

$$\zeta(t_i, L) = \int_0^{d_{tot}(t_i)/2} e^{-\frac{z}{L}}\, dx. \tag{22}$$

Eq. (21) can then be simplified to a root-solving problem of the form

$$\ln(T_i) + 2\sigma(E)\rho_0\zeta(t_i, L) = 0. \tag{23}$$

For the scenarios in which the unknown is either $\sigma(E)$ or ρ_0, Eq. (23) is linear and can be re-arranged into the semi-analytical expressions

$$\sigma(E) = -\frac{\ln(T_i)}{2\rho_0\zeta(t_i)} \tag{24}$$

$$\rho_0 = -\frac{\ln(T_i)}{2\sigma(E)\zeta(t_i)}, \tag{25}$$

which are "semi-analytical" because $\zeta(t_i, L_i)$ is still calculated by a numerical integral. In this case where scale height, L, is the unknown, Eq (23) is a nonlinear equation of the form $f(L_i) = 0$ and can be solved with the Newton-Raphson method.

In order to Newton's method, we simulated X-ray data by adding gaussian-distributed noise to the expected transmittance model. In the range where transmittance (T) is $0.01 < T < 0.9$, we scaled each of the transmittance data point by a factor α, which was randomly chosen from a normal distribution with a mean of 1.0 and a standard deviation of 0.05. Figure 12 shows a plot of the simulated horizon crossing data.

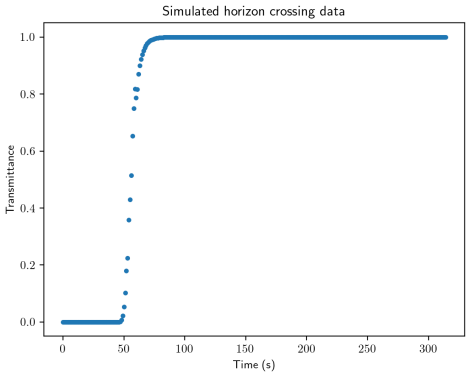

FIG. 12: Simulated transmittance data for a horizon crossing which contains gaussian-distributed noise for $0.01 < T < 0.9$.

Newton's method is described by the following iterative equation

$$L' = L - \frac{f(L)}{f'(L)}, \tag{26}$$

which is iterated until an accuracy of 10^{-4} for L is achieved. Since $f(L)$ does not have an analytical derivative, I used the secant method to evaluate $f'(L)$ with a forward difference.

Within the horizon crossing of Figure 12, I used Newton's method to calculate the value of L_i for each data point at the time t_i where $0.01 < T < 0.9$. Figure 13 shows the results of Newton's method. As shown in the plot-legend of Figure 13, the calculated value of L is $\sim 0.1\%$ different from the expected value of 8.5 km, and the maximum percent error for a single data point is $\sim 2\%$. All of this error is due to the noise in the simulated data, and L would be accurate up to the accuracy of $\zeta(t_i)$ $(\sim 10^{-10})$ if there were no noise in the data.

The range $0.01 < T < 0.90$ is used in this section since the error in L will shoot up if the simulated transmittance data points are larger than 1.0 near the top of the curve (this would cause a negative optical depth). For this reason, if this exact method were applied to real data, we would need to ensure that the comparison range does not include data points over 1.0 transmittance (this occurs when the measured photon intensity, I, is larger than the mean "unattenuated" intensity, I_0).

5.1. Discussion

Based on preliminary analysis, Newton's method is always well-behaved and will always converge to the cor-

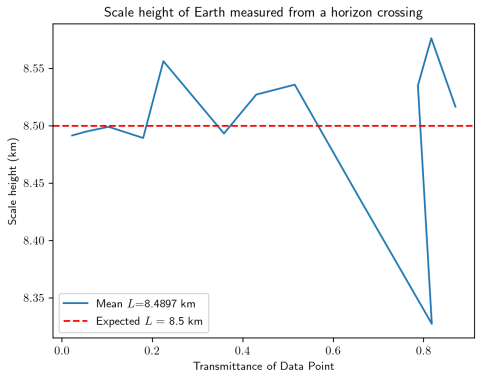

FIG. 13: Results of Newton's method when calculating L for the range of times in which the model transmittance curve is between 1% and 90%.

rect scale height. For an initial guess of $L_0 = L_{best} + 1$ km, where $L_{best} = 8.5$ km is the expected scale height, Newton's method converged in ∼7 iterations, and for an initial guess of $L_0 = L_{best}+40$ km, Newton's method converged in ∼25 iterations. Physically, Newton's method is well-behaved because a change in scale height produces a linear translation of the transmittance curve left or right on the time axis. Figure 14 shows how a model transmittance curve is altered when L is scaled by a multiplicative factor, β. If χ^2 between the transmittance data and models with different L values were calculated, the χ^2 plot would look similar to $y = x^2$ and only have a single minimum value. If the χ^2 plot were to have more than one minimum, the convergence of Newton's method to the correct scale height would depend more strongly on the initial guess L_0. However, for the algorithm presented in this paper, L_0 does not need to be a "good" guess.

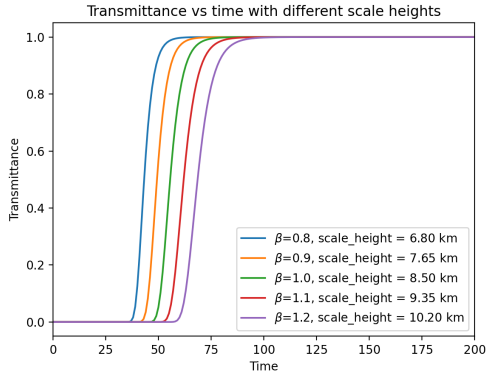

FIG. 14: Transmittance vs time for the "Standard LEO" for varying atmospheric scale heights.

In the formulation of the root-finding problem where ρ_0 and L are known, and the goal is to solve $\sigma(E)$, the direct application of Eq. (24) makes an assumption that will lead to errors in the measurement of $\sigma(E)$. The incorrect assumption is that there is a single energy, E, that defines $\sigma(E)$. In real life, transmittance data can only be collected for an *energy band*, for which E is defined as the mean energy of the energy band. Since photo-electric cross section can change significantly within a single energy band ($\sigma \propto E^{-3}$), especially below 3 keV, this could add additionally uncertainty to the measurement of $\sigma(E)$ [5]. The error related to $\sigma(E)$ not being a constant could also affect the other two problems when solving for ρ_0 and L. One solution to this problem is to only analyze X-rays above 3 keV where photoelectric cross section does not vary with energy as strongly, and/or to analyze smaller energy bands. However, both of these options reduce the signal-to-noise ratio of the data, and thus increase the error of any measurements.

6. CONCLUSION

In this paper, we introduce a *toy model* for a simplified, two-dimensional horizon crossing. This model can be extremely important in the development of HCNM and X-ray horizon crossing analysis in general, as it provides a simple way to alter atmospheric parameters, evaluate the performance of existing numerical methods, and test novel numerical methods. For an orbit similar to that of the International Space Station (ISS), a circular Earth-orbit at an altitude of 420 km, we found that a step size of ∼17 km is ideal for a horizon crossing when using an integration scheme similar to Simpson's method. The adaptive quadrature method used in this analysis is not the most computationally efficient, especially in Python, and it should only be used for providing inspiration for other algorithms. Furthermore, we introduced an algorithm that uses Newton's method to solve for atmospheric scale height from X-ray transmittance data, "data" which is simulated in this paper. In contrast to scale height, atmospheric cross section and surface-level density are uniquely determined by a linear equation and can be solved directly. Although the two numerical methods introduced in this paper are demonstrated for an ISS-like orbit, the analysis can be repeated for an arbitrary planet, an arbitrary exponential atmosphere, and an arbitrary circular orbit (Python code in Appendix C).

In Appendices 1 and 2, we consider additional possible future directions. Appendix 1 introduces non-dimensional parameters that could be used to analyze horizon crossings around different planets with different atmospheres. These non-dimensional parameters could be used, for example, in conjunction with the adaptive step size method to obtain a general relationship for the step size required for a wide range of planetary atmospheres. Appendix 2 considers a formulation of X-ray absorption in time, which is insightful to the horizon crossing, but may not have direct application, as it predicts X-ray transmission at the tangent point, not along the entire line of sight.

7. ACKNOWLEDGEMENTS

Thank you to Daniel Grin for guiding me through this project and helping to formulate new methods of analysis. Thank you to Andrea Lommen for discussing this project and sharing ideas.

Appendix A: Convergence of Gaussian Quadrature

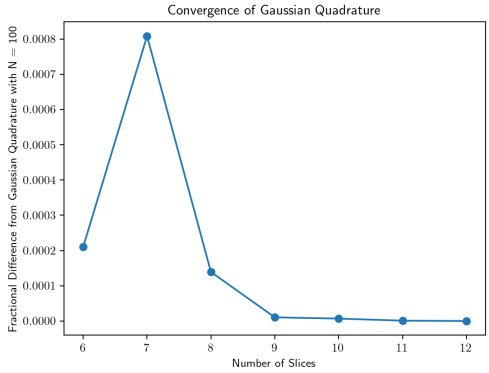

FIG. 15: Convergence of gaussian quadrature plotted against the number of quadrature points used when integrating each telescopic line of sight.

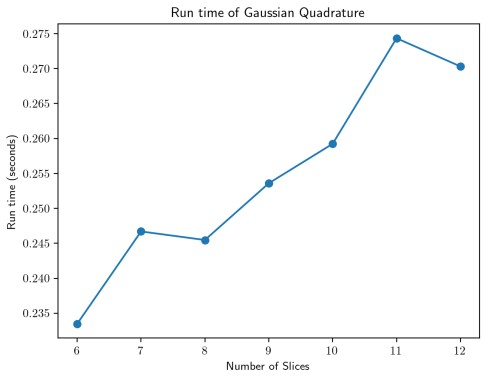

FIG. 16: Run-time of calculating a full transmittance curve with multiple gaussian quadrature methods with a range of quadrature points.

Appendix B: Ideas for future work

Throughout this project, I have explored a couple different methods of analyzing horizon crossings which could be helpful as we consider horizon crossings around different planets, two of which are explained in the following Sections.

1. Dimensionless Parameters

Dimensionless parameters offer us the opportunity to understand the similarities and differences between horizon crossings around different planets. Additionally, the use of dimensionless parameters can provide insight into how numerical techniques, such as the integration of the line of sight, must be adjusted to achieve the same performance around different planets. According to the Buckingham Pi Theorem, two dimensionless numbers are required to describe the horizon crossing as formulated in the previous sections. The first is a non-dimensional altitude, which can be defined as

$$h^*(t) = h(t)/L. \tag{B1}$$

The second is a non-dimensional "mean free path", which is defined as

$$\lambda^*(E,t) = \sigma(E)\rho_0 h(t). \tag{B2}$$

The slope of a plot of λ^* vs h^* is a constant R^* which is a property of the atmosphere:

$$R^* = \frac{\lambda^*}{h^*} = \sigma(E)\rho_0 L. \tag{B3}$$

2. Formulation in Time

A formulation of Beer's law in time may potentially provide a novel method to explore atmospheric parameters. However, this can only be achieved by considering the "transmission coefficient" at the tangent point, which is not a parameter that we would obtain from telescopic data, so it may not be as practical as predicting the full transmission for a line of sight. Nevertheless, it is an interesting problem to consider and can provide insight into the horizon crossing.

The differential equation of Eq. (1) can be transformed into a differential equation in time that predicts intensity at the tangent point, since at this point, $z(t_i) = h(t_i)$. Using the chain rule, we have

$$\frac{dI}{dt} = \frac{dI}{dx}\frac{dx}{dt}. \tag{B4}$$

Taking the derivative of Eq. (9), we can define

$$\beta(t) = \frac{dx}{dt} = \frac{2(R+h(t))}{\sqrt{R_{orbit}^2 - (R+h(t))^2}} \cdot \frac{dh(t)}{dt}, \tag{B5}$$

which simplifies to

$$\beta(t) = \frac{2R_{orbit}\omega(R+h(t))}{\sqrt{R_{orbit}^2 - (R+h(t))^2}}. \tag{B6}$$

The differential equation thus becomes

$$\frac{dI}{dt} = [\sigma(E)\rho_0 e^{-h(t)/L}\beta(t)]I = -\kappa(t)I \tag{B7}$$

where $\kappa(t) = \sigma(E)\rho_0 e^{-h(t)/L}\beta(t)$. The solution to this differential equation gives the transmission coefficient of the tangent point as a function of time,

$$T_h(t) = e^{-\kappa(t)t}. \tag{B8}$$

Appendix C: Note on Code

All code is located in the github repository https://github.com/dgrin1/nruhl_hw, in the folder "nruhl_final_project/". The following list enumerates the locations of certain functions and scripts in the repository.

1. Figures in Section 4.1 are from Results/los_thickness.py
2. Adaptive quadrature is executed in the script AnalyzeCrossing.py
3. Plots related to convergence of adaptive quadrature are from quadapt_convergence.py
4. Plots related to convergence of gaussian quadrature are from gauss_convergence.py
5. Plots related to nonlinear equation solving are from Results/nonlinear_solver_scaleheight.py
6. The plot of transmittance vs time for different atmospheric scale heights is made in Results/modify_params.py
7. Work on dimensionless numbers is located in Experimental/pi_numbers.py and other scripts in Experimental/
8. Planet ephemeri are located in PlanetEphems/

[1] R. G. Roble and P. Hays, Planetary and Space Science **20**, 1727 (1972).

[2] G. R. Smith and D. M. Hunten, Reviews of geophysics **28**, 117 (1990).

[3] J. R. Determan, S. A. Budzien, M. P. Kowalski, M. N. Lovellette, P. S. Ray, M. T. Wolff, K. S. Wood, L. Titarchuk, and R. Bandyopadhyay, Journal of Geophysical Research (Space Physics) **112**, A06323 (2007).

[4] K. S. Wood, J. R. Determan, P. S. Ray, M. T. Wolff, S. A. Budzien, M. N. Lovellette, and L. Titarchuk, in *Optical Spectroscopic Techniques, Remote Sensing, and Instrumentation for Atmospheric and Space Research IV*, edited by A. M. Larar and M. G. Mlynczak (2002), vol. 4485 of *Society of Photo-Optical Instrumentation Engineers (SPIE) Conference Series*, pp. 258–265.

[5] N. C. Ruhl, A. N. Lommen, N. H. Schwab, R. M. Hladky, K. S. Wood, and P. S. Ray, Proceedings of the AAS Guidance, Navigation, and Control Conference, Paper AAS 22-073 (2022).

[6] S. I. Sheikh, D. J. Pines, P. S. Ray, K. S. Wood, M. N. Lovellette, and M. T. Wolff, Journal of Guidance, Control, and Dynamics **29**, 49 (2006).

[7] C. Elachi, *Introduction to the Physics and Techniques of Remote Sensing*, Wiley Series in Remote Sensing (John Wiley & Sons, New York NY, 1987).

[8] S. C. Chapra and R. P. Canale, *Numerical Methods for Engineers, 7th ed.* (McGraw-Hill Education, 2 Penn Plaza, New York, NY 10121, 2015).

[9] M. Newman, *Computational Physics; Revised and Expanded* (University of Michigan, 2013).